Debris flow hazard mitigation: A simplified analytical model for the design of flexible barriers

Debris flow hazard mitigation: a simplified analytical model for the design of flexible barriers

Roberto Brighenti[1], Andrea Segalini*[1], Anna Maria Ferrero[2]

[1]*Dept. of Civil-Environmental Engineering and Architecture, University of Parma, Viale G.P. Usberti 181/A - 43100 Parma – Italy, Ph. +39 0521 905910, Fax +39 0521 905924*

[2]*Dept. of Earth Science, University of Turin, Via Valperga Caluso 35 – 10135 Torino – Italy, Ph. +39 011 6705114*

* E-mail: *andrea.segalini@unipr.it*

Abstract

A channelized debris flow is usually represented by a mixture of solid particles of various sizes and water flowing along a laterally confined inclined channel-shaped region to an unconfined area where it slows down and spreads out into a flat-shaped mass.

The assessment of the mechanical behavior of protection structures upon impact with a flow, as well as the energy associated to it, are necessary for the proper design of such structures which, in densely populated areas, can prevent victims and limit the destructive effects of such a phenomenon.

In the present paper, a simplified analysis of the mechanics of the impact of a debris flow is considered in order to estimate the forces that develop on the main structural elements of a deformable retention barrier.

For this purpose, a simplified structural model of cable-like retention barriers has been developed - on basis of the equation of equilibrium of wires under large displacement conditions, - and the restraining forces, cable stresses and dissipated energies have been estimated.

The results obtained from parametric analyses and full-scale tests have then been analysed and compared with the proposed model.

Keywords: *Debris-flow, Barriers, Cable structure.*

Nomenclature

A	Cross section of a horizontal cable
A_t	Cross section of an equivalent cable representing the transversal net
$d(t)$	Depth of a generic cable measured with respect to the upper free surface of the accumulated material
d_{ji}	Relative vertical distance between cables *i* and *j*
e	Horizontal distance between the first and the last edge of a generic cable, measured normal to the cable
E	Young's modulus of the cable
E_b, E_E	Energy dissipated by the brakes and elastic energy stored in the cables, respectively
E_t	Young's modulus of the equivalent transversal cables representing the net
$f_b, f_{b,\max}$	Generic force and maximum allowable force in the brake
$h(t)$	Height of the accumulated material at generic time *t*
h_B	Total height of the barrier
h_0	Constant height of the debris flow surge
H	Component along the x direction of the tension force along a cable
k, g	Earth pressure and gravity acceleration coefficients
L_i, l_i	Effective length and projected length along the x-axes of cable *i*, respectively
n	Number of horizontal cables in the barrier
p	Constant vertical distance between the horizontal cables
$Q_i(x)$	Total horizontal load acting along a generic *i*-th cable

$q_{c,j}$, q_{ic}	Horizontal load supported by cable *j* due to load $q(z_i)$ acting on cable *i* and the horizontal load supported by cable *i* when all the other cables are loaded by $q(z_j)$
$q_d(x)$	Horizontal load due to the dynamic pressure on the barrier
$q_s(d,x)$	Horizontal load due to the static pressure on the barrier at depth *d*
$q(z_i,t)$	Horizontal load, at time *t*, acting directly on the cable located at vertical co-ordinate z_i
$s_b, s_{b,\max}$	Generic displacement and maximum allowable displacement in the brake
t	Generic time instant
$r(z_j,z_i)$	Function defining the horizontal ratio between the displacements of cable *i* and cable *j* (placed at vertical coordinates z_i and z_j, respectively)
$T(x,d)$	Tension force along a cable (in a point having co-ordinate *x*) placed at the depth *d*
$u(x)$	Horizontal displacement of a generic point, with co-ordinate *x*, of the cable (in the *y* direction, as shown in Figure 5)
$\bar{u} = u(x = l/2)$	maximum displacement of the cable, which occurs at its midpoint
V	Components in the *y* direction of the reaction forces acting at the cable edges
v_0	Arrival velocity of the debris flow
z	Generic vertical co-ordinate of the horizontal cable
z_i	Generic vertical co-ordinate of the *i*-th horizontal cable
α	Empirical coefficient for dynamic pressure estimation
ρ_d	Mass density of the debris flow
θ	Inclination angle of the slope
Fr	Flow rate of the debris [m^3/s]

α	Average inclination of the debris deposition behind the barrier
μ	Interface friction coefficient between landslide debris and deposited debris
T_f	Duration of impact [s]

1. Introduction

Debris flows are rapid mass movements, composed of a mixture of grains, water and air, that develop under the effect of gravitational forces. The amount of energy involved in such phenomena is enormous and their mobility is such that it allows them to propagate for several hundreds of meters without losing their destructive potential. Owing to these characteristics, debris flows have been ascribed as being among the most dangerous and catastrophic of natural events [1]. The above cited phenomenon generally originates from collapses (landslides, erosions, etc.) associated with heavy precipitations due to extreme meteorological events such as heavy rainfall or rapid snowmelt. The characteristics that identify a debris flow are:

- A mixture of water and sediments (including sometimes vegetation debris);
- Unstable and non-uniform flow behaviour;
- High velocity of the mobilized mass and strong impact forces;
- Sudden phenomena of short duration.

Govi et al. [2] found, on the basis of a large number of observations that most of these phenomena generate in small to medium scale hydrological basins (up to 13 km^2), around 40% of the observed phenomena develop along channels having a with a steeper slope than 35° and more than 40% of the occurrences have a recurring time of over 50 years. Several classification of these phenomena have been proposed by various authors (Pearson & Costa [3]; Costa [4]; Phillips & Davies [5]; Meunier [6]; Wan & Wang [7]; Coussot & Meunier [8]; Hungr et al. [9]; Takahashi [10]). The study of these phenomena is very difficult due to their short duration and unpredictability, the lack of historical data for a given basin and the complexity of the involved mechanical phenomena. Post event surveys allow some of the depositional features to be identified and provide indications on the maximum flow height. However, they lack information on the development of the phenomena with time. For this purpose, recursive events have been monitored out by several authors (Okuda et al. [11]; Marchi et al. [12]; Hürlimann et al. [13] ; Tecca et al. [14]). Most of the studies, which had the aim of determining of the characteristic features of a debris flow, have been carried out in artificial channels, where the main involved variables were measured and others were controlled during the tests (Takahashi [10]; Iverson [15]). However, some uncertainties have

remained and other scaled models have been developed to simulate deposition mechanics (Mizumaya and Uehara [16]; Liu et al. [17]; Chau et al. [18]; Deganutti et al. [19]; Ghilardi et al. [20]; Major [21]) but also to analyze transportation mechanics and energy dissipation [21]. Iverson [15] demonstrated that the uncertainties and difficulties in the interpretation of the experimental results are due to scale effects and to an incorrect artificial reproduction of natural phenomena.

In this work, a simplified structural model, developed by the Authors for the safety assessment of retention barriers against channelized debris flows, is presented and some parametric cases and a full scale test on debris flow barriers is interpreted through the proposed approach. This model has been developed as a simplified and efficient tool that can be used to verify of the supporting cables and foundations of a flexible debris flow barrier.

The present analytical and numerical-based approach has a different aim then that of a Finite Element Model (FEM). The numerical approach to the problem using 3D FEM is in fact a well-known tool in this context (Ferrero [22]). However, computational experience using FEM modeling for these kinds of structures has shown that a large amount of time is needed for the geometrical setup of the model and several numerical instabilities develop due to the non linearity of the problem. The great effort required by FEM for this kind of problem limits the possibility of investigating different geometrical configurations, load schemes etc. It is in fact suitable to represent a specific configuration but does not allow investigation to be made of the influence of debris flow parameter modification (flow height and velocity, debris density etc.). On the other hand, parametrical analyses are common practice in geotechnical design because the aforementioned reasons. Consequently, the Authors decided to develop a simplified method (which is not yet available to our knowledge) that would allow several parametrical analysis to be performed in a limited time. Parametrical analysis should take into account the physical and mechanical features of debris flow which usually vary during debris development and which are consequently difficult to define in a deterministic way. It should be noted that no consideration has been given to the mechanical and physical behavior of debris flows in this paper. The proposed model involves the input parameters being acquired through a preliminary characterization of the design event. However, if the proposed tool

is adopted, the designer will be able to perform sensitivity analysis that will help to quantify the influence of parameter variability.

2. Debris flow mechanics

As already mentioned in the introduction, a detailed description of the complex mechanics of a debris flow is not the scope of this paper. This aspect has been studied by several authors considering the different phases that can be identified the debris flow development: the triggering phase [23], the run out phase (e.g. Hungr and Evans [24]; Pirulli [25], Takahashi [10]) and the deposition phase (Major [21], Vallance [26]). However, for the scope of this work, the most relevant aspect is the run out phase and, in particular, the determination of its velocity, volume and discharge rate, since debris flow impact power is connected to its kinetic energy, and to the energy dissipation effects during motion (Cesca [27]).

The velocity of a debris flow during its run out depends on several factors, such as: dip of the slope, the water mixture content, the grain distribution etc.. All these factors determine the relationship between the induced internal stresses and the deformation in relation to the applied external stresses, which is usually known as fluid rheology. Since the debris flow is a multi-phase mixture of different materials, its rheology somewhere falls in between the mechanical elastic behavior of the solid phase and the viscous behaviour of the liquid phase. All these aspects determine the kind of motion regime of the debris, which is mainly ruled by both inertia and viscosity forces. The well-known Bagnold number, determined in one of the pioneer works on debris flow rheology carried out by Bagnold [28], is the ratio between these two components (inertia and stresses due to viscosity) and can be used to identify different motion regimes. Bagnold used the term “macroviscous” to indicate a linear regime that is characterized by small Bagnold numbers, in which the shear stresses behave as in a Newtonian fluid with a corrected viscosity, and the term “grain-inertia” to indicate a regime that is characterized by large Bagnold numbers, in which the stresses are independent of the fluid viscosity but dependent on the square of the shear rate and on the square of the granular-phase concentration.

A rheological regime, usually termed “collisional”, which is based on the interaction between particles, during which momentum is exchanged and energy

is dissipated because of inelasticity and friction, has recently been defined (Goldhirsch [29], Jenkins and Hanes [30]; Hanes [31]).

Armanini et al. [32] have shown how as both regimes can be simultaneously present in a debris flow: the behaviour can be reproduced by the kinetic theory in the proximity of the free surface, where the particle concentration is relatively small, while a layer dominated by frictional contacts can be observed near the static bed.

The study of debris flow strains and displacements is conveniently analysed considering three fundamental physical principles: mass, energy and momentum conservation, which lead to the driving equations. The above equations can be solved using several different methods: those based on continuum mechanics (i.e. the heterogeneous real mass is treated as a continuum) have been widely and successfully applied (e.g. Chen and Lee [33]; Denlinger and Iverson [34]; McDougall and Hungr [35]).

When the debris thickness is far smaller than its extent (measured parallel to the bed), averaged depth Saint Venant equations can be used because the debris composition can reasonably be considered constant in a section, due to the limited height, thus avoiding the necessity of a complete 3-dimensional description of the flow (Savage and Hutter [36]).

The design of barriers against debris flows is based on the impact forces that are determined by the sum of the dynamic pressure (which can reach values up to the order of 10 KN/m^2) and of the particle collision (which is characterized by values of 100 KN/m^2 or more) (Suwa and Okuda [37]).

The dynamic impact can theoretically be estimated assuming an incompressible fluid hypothesis against a rigid barrier, and can be the assessed on the basis of momentum conservation for a steady fluid motion (Hungr [38]; Van Dine [39]) while a theoretical solution for cable-like retention barriers is still not available.

2.1 Forces induced by debris-barrier impact

The pressure produced by the impact of a debris flow on the barrier can be estimated considering both the dynamic impact pressure and the static pressure of the deposited debris (Kwan & Cheung [40]). The former can be determined considering the well-known Bernoulli theorem; the kinetic energy of the flowing material, $\rho_d \cdot v_0^2 / 2$, is in fact into a pressure load when the velocity vanishes due

to the impact. The dynamic pressure on the barrier can thus be estimated as (Fig. 1a):

$$q_d(x) = \alpha \cdot \rho_d \cdot v_0^2 \tag{1}$$

where α is an empirical coefficient that varies between 1.5 and 5, according to Canelli et al. [41] and which can be assumed to be equal to 2.0 when the barrier is flexible and drained, the flow regime is granular and there is a lack of site specific information, where ρ_d, v_0 are the density and the impact velocity of the debris, respectively. Studies have been carried out to back analyze some natural debris flow phenomena that have impacted monitored barriers [42] using a multi-stage surge model. However, some of the parameters involved in the analysis were estimated (i.e. the lateral earth pressure coefficient, the density of the debris, etc.) while others were measured directly (i.e. front velocity, surge height, etc.). An extensive analysis on design approaches for debris resisting barriers has been presented by Kwan & Cheung [40].

Generally, the debris could hit the barrier in the form of surges which fill the barrier either continuously or intermittently; the most critical impact scenario on barrier stability should always be chosen [40].

The thickness (h_0) and velocity (v_0) of moving debris surges can be estimated from debris mobility models using appropriate rheological parameters such as those recommended by Lo [43]. On the other hand, when the debris starts to accumulate behind the barrier, a static pressure can be assumed to occur (Fig. 1). The height of the accumulated material at the generic time t can be estimated, as shown in Eq. (2), by equating the volume of the material that arrives after such a time interval from the slope and the volume of the accumulated material behind the barrier (Fig. 1), (time t=0 is assumed when the first particle of the debris-flow impacts the barrier) as:

$$h(t) = \sqrt{2 \cdot v_0 \cdot t \cdot h_0 \cdot tg\theta} \tag{2}$$

In the above relation h_0, θ are assumed to be the constant height of the debris flow surge and the inclination of the slope behind the barrier, respectively. It should be noted that, in order to use Eq. (2) it is necessary that $\theta > 0$. The static pressure acting at depth $d(t)$, measured with respect to the upper free surface of the material (Fig. 1b), can be assessed through the relation reported in Eq. (3), as

usually occurs in geotechnical science for the assessment of the static pressure produced at a given depth:

$$q_s(d) = k \cdot d(t) \cdot \rho_d \cdot g = k \cdot \underbrace{(h_0 + h(t) - z)}_{d(t)} \cdot \rho_d \cdot g \tag{3}$$

where k, g are the earth pressure coefficient and the acceleration of gravity, respectively, while z is the vertical position of the point under consideration (Fig. 1b).

By considering the barrier made up of *n* horizontal supporting cables -in the following assumed to be placed at a constant relative distance of $p = h_B/(n-1)$ for the sake of simplicity the pressure load $q_i(z_i)$ (assumed to be constant along each horizontal cable) acting on the *i*-th cable located at the vertical co-ordinate $z_i = h_B \cdot (i-1)/(n-1) \geq h_0$ can simply be calculated as in Eq. (4) (the cables are numbered starting from 1 at the bottom of the barrier),

$$q(z_i \geq h_0, t) = \begin{cases} 0 & t < t_1 = (z_i - h_0)^2/(2v_0 h_0\, tg\theta) \\ q_d = \alpha \cdot \rho_d \cdot v_0^2 & t_1 \leq t \leq t_2 = z_i^2/(2v_0 h_0\, tg\theta) \\ q_s = k \cdot \left[h_0 + h(t) - h_B \cdot \dfrac{(i-1)}{(n-1)} \right] \cdot \rho_d \cdot g & t > t_2 \end{cases} \tag{4}$$

while Eq. (5) should be used when the *i*-th cable is located at vertical coordinate $z_i < h_0$

$$q(z_i < h_0, t) = \begin{cases} q_d = \alpha \cdot \rho_d \cdot v_0^2 & t < t_1 = z_i^{\,2}/(2v_0 h_0\, tg\theta) \\ q_s = k \cdot \left[h_0 + h(t) - h_B \cdot \dfrac{(i-1)}{(n-1)} \right] \cdot \rho_d \cdot g & t \geq t_1 \end{cases} \tag{5}$$

In others words, Eqs (4) and (5) enable one to evaluate the pressure exerted directly on a given cable located at coordinate z_i, once its position with respect to the flowing material and to the accumulated material is known. Eq. (4) is valid for cables located at a greater height than the thickness of the flowing debris at different time intervals: the cable is not yet in contact with the debris material for $t < t_1 = (z_i - h_0)^2/(2v_0 h_0\, tg\theta)$ and it is therefore unloaded; for the $t_1 \leq t \leq t_2 = z_i^2/(2v_0 h_0\, tg\theta)$ interval the i-th cable falls inside the portion of the barrier that impacts with the flowing debris while the cable for $t > t_2$ is in contact with the material at rest behind the barriers. Similarly, Eq. (5) allows one to

estimate the pressure on a cable located at a coordinate z_i which is lower than the thickness of the flowing material.

Since the cables are placed at a constant vertical distance of p , the distributed load (assumed, for the sake of simplicity to act in a horizontal plane) acting on a single cable of unit horizontal length is given by Eq. (6)

$$q_t(z_i,t) = q_t(d,t) = \begin{cases} p \cdot q(z_i,t)/2 & i = 1, n \\ p \cdot q(z_i,t) & 2 \le i \le n-1 \end{cases} \tag{6}$$

The above and following relations are obviously not restricted by the hypothesis of a constant *p*. More general relationships can be obtained for variable relative cable distances. However, for the sake of analytical simplicity, such a hypothesis has been introduced to illustrate the analytical model.

While calculating the pressure acting on the barrier, the model does not take into account the deformation induced by the pressure exerted by the flowing granular material; since the case of a rigid barrier is the most critical in the design of such retention structures, the mitigation of the pressure, due to the barrier deformation, can reasonably be neglected from the safety point of view. This hypothesis holds true since the maximum transversal displacement of the barrier, as inferred from both experimental and numerical results, is usually much lower (10 - 15%) than the barrier extension (see Par. 4.2).

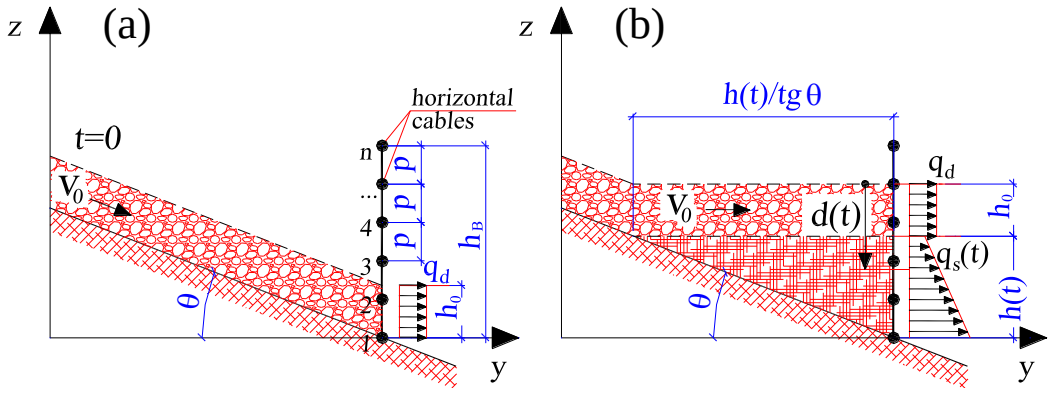

Fig. 1. Debris accumulation behind the barrier and corresponding loads at a generic time instant.

The assumption of a constant load along the cable is an acceptable simplification from the engineering safety point of view; this hypothesis allows one to treat the problem as a two dimensional one, characterised by governing equations that can

easily be handled for a simplified design of the retention barrier, as will be shown hereafter.

3. Mechanics of cable-like retention barriers

A simplified structural model for the assessment of the forces that develop in the retention barrier against a channelized debris flow can be formulated taking into account the typical structural lay-out of such elements.

The typical channelized debris flow barrier has an almost trapezoidal shape and is anchored to the ground (generally at the channel sides) by means of grouted anchors or cables. The main structural cables are horizontal and their number depends on the overall height and on the expected flow parameters (Fig. 2).

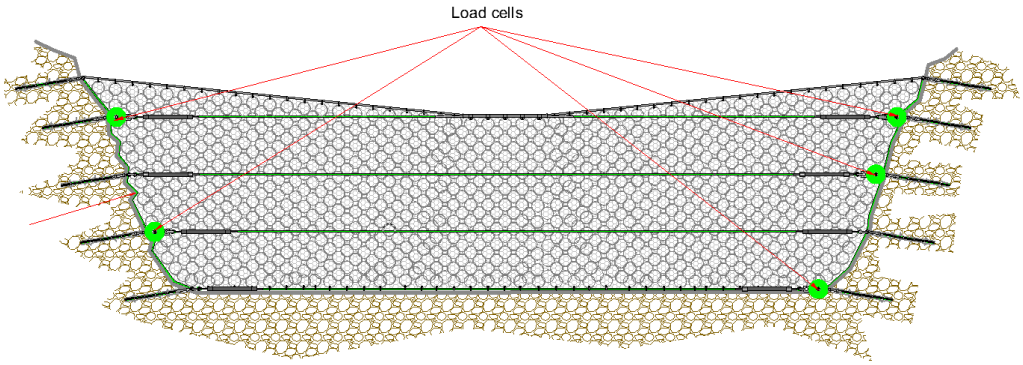

Fig. 2. Typical structural lay-out of a net retention barrier against debris-flow. The single element features and the geometrical lay-out can vary according to the make and model of the barrier and to particular installation conditions (channel size, depth, etc.). The load cells referred to here are those that were used during on site tests carried out at the Pieve di Alpago (BL, Italy) test site (see Section 4).

To each horizontal cable can be connected a dissipating element that would limit the amount of force transferred to its foundations during the debris flow impact (Fig. 3).

The structural net is typically formed by interconnected steel rings of homogeneous diameter (typically 30-50 cm); sometimes another net with smaller diameter openings is overlaid to the first one to retain smaller debris particles.

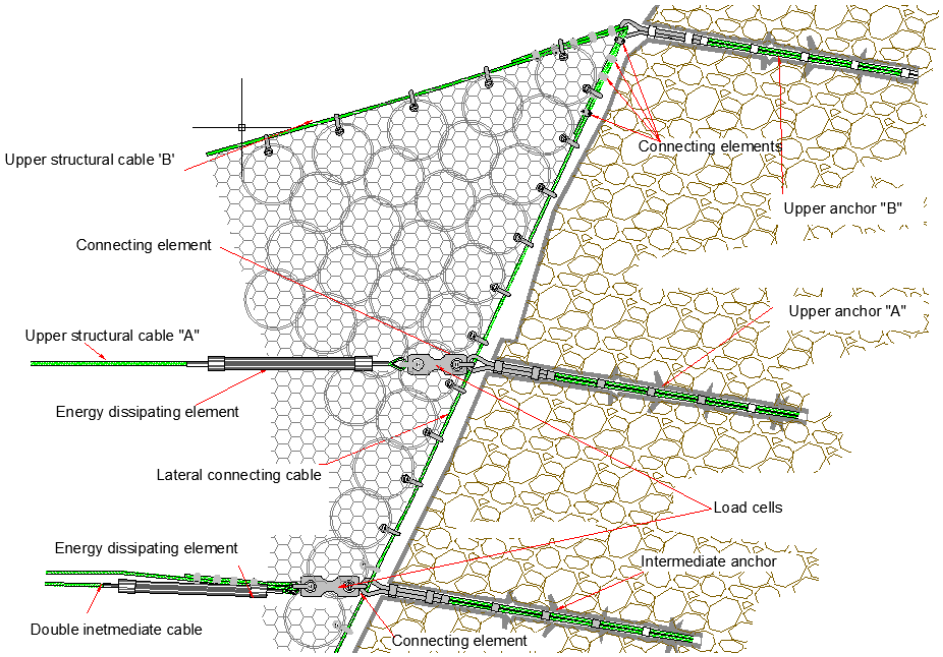

Fig. 3. Particular of the barrier foundations, dissipating elements and supporting cables. Single elements are variable with the make and model of the barriers available on the market.

Fig. 4. Example of a debris flow barrier (installed at the Pieve di Alpago (BL, Italy) test site, see Section 4).

From the observation of Fig. 2 it can be noted that the main resisting elements are the horizontal cables fixed at their extremities to the foundations, while the net has

the role to retain the flowing solid particles and to transmit the developed forces to the above described cables.

The governing equation of the equilibrium of a loaded cable can be usefully employed to describe the mechanical behaviour of such a structural system.

Let us consider the barrier constituted by several horizontal cables mounted at a reciprocal constant distance equal to p. The i-th cable - having its extremities fixed at the points A and B - is characterized by a horizontal length equal to l_i, while its total effective length (when elongated under loading) is assumed to be equal to L_i (Fig. 5). The distributed load acting on such a cable is assumed to lie in an horizontal plane and to be constant with respect to the x co-ordinate at a fixed time t. The load is, however, variable with time, since the depth $d(t)$ of the cable with respect to the top surface of the flowing material increases with t (Fig. 1b).

3.1. Formulation of the equilibrium equation of a cable-like structure

The present model, for sake of simplicity, considers the main resisting cables to be loaded only in the horizontal direction by the forces produced by the debris impact on the barrier, while the resultant of the vertical forces transmitted by the connecting net to the single cable is considered as negligible. As a consequence, only the deformation of the cables in the horizontal plane will be assumed to be significant in the resistant mechanism of the structure.

Each cable of the barrier is assumed to have fixed extremities, i.e. the end points of the cables are prevented to displace by some foundation system which mechanical behavior is beyond the scope of the present research.

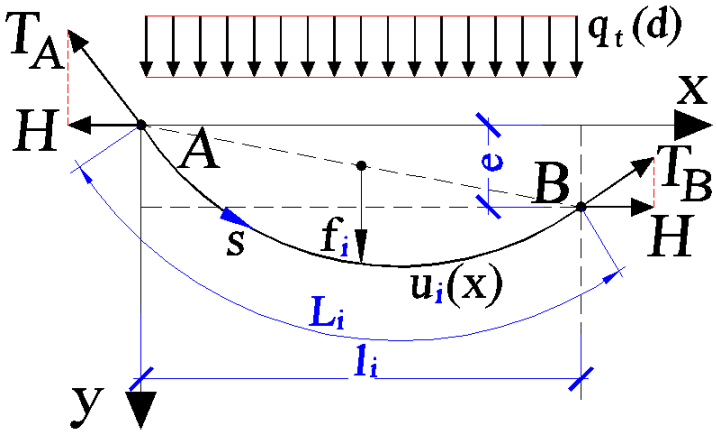

Fig. 5. Scheme of the top view of a single cable under the forces produced by the impact of a debris-flow, with related geometrical and static quantities.

Starting from the equilibrium equation (Eq.(7)) of the *i*-th cable in differential form at the time instant t [44],

$$\frac{d^2 u_i(t)}{dx^2} = -\frac{q\ (z_i,t)}{H_i} = -\frac{q_i(d,t)}{H_i} \tag{7}$$

after a double integration and by assuming a constant distributed load at a given time instant $q_i(d)$ (the dependence on time *t* for sake of brevity is not explicitly indicated in the following relations) and the two extremities of the cable to be located at the coordinates $(x, y) = (0,0)$ and $(x, y) = (l_i, \mathrm{e})$ (referred to the horizontal plane containing the cable, Fig. 5) corresponding to the points A and B, respectively, the cable equation can be explicitly written as (Levy [45]):

$$u_i(x) = \frac{q_i(d)}{2H_i}\left(x \cdot l_i\ - x^2\right) + \frac{\mathrm{e}}{l_i}x \tag{8}$$

where $q_i(d) = q(z_i = h_b - d)$ is the constant horizontal load acting along the cable under consideration placed at a depth d below the actual top free surface of the flowing material, while H_i is the constant component along the *x* direction of the tensile axial force $T_i(x)$ in the cable [44]. Such a quantity can be obtained by imposing the effective length of the cable to be equal to L_i through the equation:

$$L_i = \int_0^{l_i} \sqrt{1 + u_i{}'^2\,(x)}\ dx \tag{9}$$

which is obtained by integrating the trivial geometric relation $dL_i = \sqrt{dx^2 + dy^2} = dx\sqrt{1 + u_i{}'^2\,(x)}$ (since $dy = dx \cdot u_i'(x)$) that quantifies the length of a generic curve which shape is described through the displacement relation $u_i(x)$.

By denoting with f the quantity $f = q_{ti} \cdot l_i^2 / 8H_i$ (see Fig. 5, where the geometrical interpretation of f is represented, i.e. the maximum transversal displacement measured with respect to the straight line A-B) and expanding in

Taylor series the expression of the integrand function in Eq. (9) (the dependence on the depth d is omitted in the notation for simplicity), one can obtain:

$$L_i \cong l_i \cdot \left(1+\frac{8}{3}\frac{f^2}{l_i^2}+\frac{1}{2}\frac{\mathrm{e}^2}{l_i^2}\right)+..... \tag{10}$$

The sought term H_i, which can be demonstrated from equilibrium considerations to be independent of *x*, can be finally obtained by using Eqs (8-10):

$$H_i \cong \frac{\sqrt{3}}{6}\cdot\frac{q_i \cdot l_i^2}{\sqrt{2L_i \cdot l_i - 2l_i^2}} \tag{11}$$

where the particular case characterised by $\mathrm{e}=0$, has been considered.
The tensile force $T_i(x)$ acting along the cable can be also explicitly obtained through the following relation (Levy [45]):

$$T_i(x) = H_i \cdot \frac{ds}{dx} = H_i \cdot \sqrt{1+u_i'^2(x)} = H_i \cdot \sqrt{1+\left[\frac{q_i}{2H_i}\left(l_i - 2x\right)\right]^2} \tag{12}$$

by projecting the force H_i along the tangential direction of the cable in the point of interest or, in other words, by calculating the product $H_i \cdot ds/dx$, where s denotes the curvilinear abscissa along the cable under consideration (Fig. 5).
At the two extremities of the cable, the components of the reaction forces in the *y* direction are given by the trivial value:

$$V_i(x=0) = V_i(x=l_i) = H_i \cdot \left.\frac{du_i}{dx}\right|_{\substack{x=0\\x=l_i}} = \frac{q_i \cdot l_i}{2} \tag{13}$$

The elastic deformation of the cables under loading must be also considered in order to explicitly write the total effective length L_i; in such a case the problem is characterised by another source of nonlinearity due to the dependence of the cable length L_i on the tensile force $T_i(x)$ which depends itself on L_i.
Under limited deformation – 10-15% of the cable length - it can be assumed that the tensile force $T_i(x)$ is approximately equal to H_i (which does not depend on *x*) all along the cable, i.e. $T_i(x) \cong H_i = const.$ (since $ds \cong dx$); in such a way the effective length of the cable (assumed to obey the linear elastic Hooke's law) L_i can be written as:

$$L_i = l_i \cdot \left(1 + \frac{H_i}{E_i A_i}\right) \tag{14}$$

The limited deformation of each cable is considered in order to maintain the appropriate functionality of the structure. According to Kwan & Cheung [40] the deformable barrier should sustain structural integrity for a deformation in the direction of the debris impact not lower than 10% of its total length and, in order to retain a considerable amount of material behind its deformed shape, it is suggested that the final deformation should not be greater than 15% of its total length.

The last relation used together with Eq. (11) allows to calculate – by solving the obtained non-linear problem – the effective cable length and the corresponding force H_i at the equilibrium state. The above assumption can be justified by considering that even for a cable having a noticeable transversal deformation such as $f = 0.1 \cdot l_i$, its effective length is $L_i \cong 1.027 \cdot l_i$ (see Eq. (10)) and the axial force value along the cable lies in the range $H_i \le T_i(x) \le 1.08 \cdot H_i$ (obtained by using Eqs (11) and (13)), while for $f = 0.2 \cdot l_i$, $L_i \cong 1.107 \cdot l_i$ and $H_i \le T_i(x) \le 1.28 \cdot H_i$. It must be also recalled that, in debris flow net barriers, the presence of brakes is quite common; such a devices operate by dissipating energy and by increasing the cable length once the maximum allowable force of the brake is reached. Such an increased length produces a beneficial effect by inducing a decrease of the tension forces in the cables, while neglecting the brakes usually leads to a conservative design of the barriers. Such a topic will be discussed in Sect. 3.3 where the brakes modelling is presented.

The maximum displacement of the *i*-th cable occurring at its midpoint in the particular case $\mathrm{e} = 0$, is equal to $\bar{u}_i = u_i(x = l_i/2) = q_i \cdot l_i^2 / 8H_i$ (see Eq. (8)). The relation between the distributed load q_i and such a maximum displacement can thus be written from the solution of the equations below:

$$q_i(\bar{u}_i) = \frac{8H_i \cdot \bar{u}_i}{l_i^2} \tag{15}$$

$$\text{with} \qquad H_i \cong \frac{\sqrt{3}}{6} \cdot \frac{q_i \cdot l_i}{\sqrt{2}\sqrt{\left(1+\frac{H_i}{E_i A_i}\right)-1}} \rightarrow H_i = \left(\frac{q_i^2 \cdot l_i^2 \cdot E_i A_i}{24}\right)^{1/3}$$

where the relation for the approximate cable effective length evaluation (Eq. 14), has been used together with Eq. (11); finally the sought relation $q_i(\bar{u}_i)$ (see Eq. (15_1)) can be explicitly obtained:

$$q_i(\bar{u}_i) = \frac{64 E_i A_i}{3 l_i^4} \cdot \bar{u}_i^3 \tag{16}$$

3.2. Effect of the net connections between cables

Since the horizontal cables are connected by the barrier net, it can be assumed that they are joined together by 'equivalent' vertical cables having the effect to distribute a portion of the load directly applied to each horizontal cable to the adjacent ones (Fig. 6a). The differential equilibrium equation Eq. (7) for the *i*-th horizontal cable can thus be modified as:

$$\frac{d^2 u_i}{dx^2} = -\frac{q_i(x) - q_{ic}(x) + q_{ci}(x)}{H_i} = -\frac{Q_i(x)}{H_i} \tag{17}$$

in which $q_{ic}(x), q_{ci}(x)$ represent the portion of the "direct" load $q_i(x)$ acting on cable *i* transferred to the adjacent cables and the "indirect" loads transmitted to the cable *i* from the other loaded cables, respectively, i.e.:

$$q_{ic}(x) = \sum_{\substack{j=1 \\ j \neq i}}^{n} q_{i,j}(x), \qquad q_{ci}(x) = \sum_{\substack{j=1 \\ j \neq i}}^{n} q_{j,i}(x) \tag{18}$$

where $q_{i,j}(x)$ is the "indirect" load carried by the cable *j* when the "direct" load $q_i(x)$ is acting on the cable *i*, while $q_{j,i}(x)$ is the "indirect" load carried by the cable *i* when the "direct" load $q_j(x)$ is acting on the cable *j*.

In other words, the load $q_{ic}(x)$ represents the total fraction of the "direct" load acting on the cable i carried by all the other cables $j \neq i$, while $q_{ci}(x)$ represents the sum of the portions of the "direct" loads acting on all the other cables $j \neq i$ transferred to the cable i.

As previously stated, for sake of simplicity, it can be assumed the loads $q_i(x), q_{ic}(x)$ and $q_{ci}(x)$ to be constant along the *x*-coordinate and acting on the horizontal plane containing each cable. The problem is now to estimate the loads $q_{i,j}$ and $q_{j,i}$ in order to rewrite the equilibrium condition, given by Eq. (17), with the proper effective total transversal load $\left(q_i - q_{ic} + q_{ci}\right)$. Due to the load-maximum deflection relationship given by Eq. (16), the loads $q_{i,j}$ and $q_{j,i}$ in Eq. (18) can be evaluated once the maximum displacement $\bar{u}_{i,j}$ of the cable *j* (produced by the distributed load q_i acting on cable *i*, Fig. 6a, c) or the maximum displacement $\bar{u}_{j,i}$ of the cable *i* (produced by the load q_j acting on cable *j*, Fig. 6d) are known.

It should be recalled that, in the real case, the cables in the barrier are not only subjected to horizontal loads but also to vertical ones due to the effect of the transversal net connecting them (see Figs 2-4). In a general case, by considering a distributed load acting on a single inclined plane along the whole cable, the deflection of a single wire takes place in a plane containing the cable extremities and the load direction, i.e. the present model can still be applied but in a different plane from the horizontal one.

It must be also considered as the vertical components of the forces acting along a single cable are significant only for the uppermost one, since the lower and the intermediate cables of the barrier are usually either restrained by the channel bottom or symmetrically surrounded by other cables, with the consequence of being subjected to a simple nearly horizontal force.

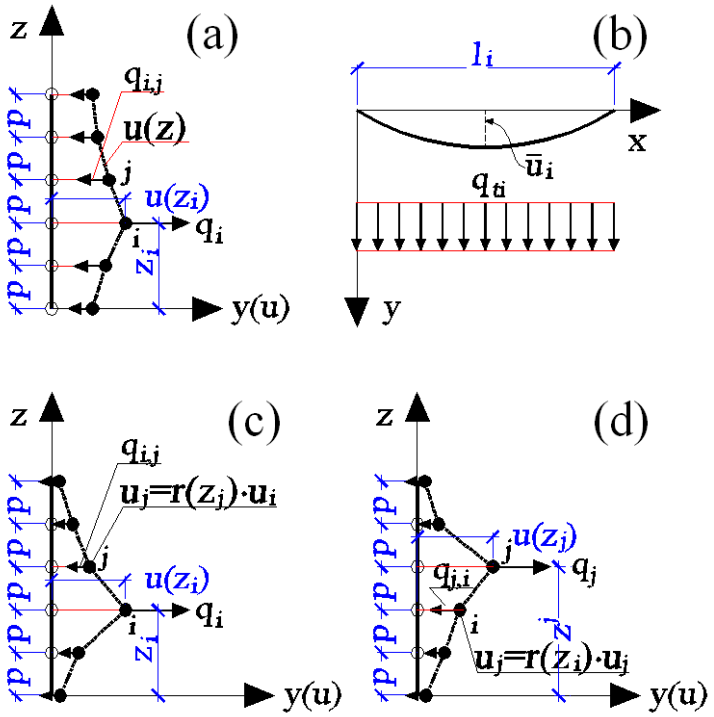

Fig. 6. Scheme of the forces developed in cables j for a load acting on the cable i (a); horizontal cable under a concentrated load (b); simplified model for the assessment of the load carried by the cables adjacent to cable i for a load q_i acting on it (c, d).

By indicating with $\bar{u}_{i,j}$ the maximum displacement occurring in cable *j* when the cable *i* shows a maximum displacement equal to $\bar{u}_i$, an influence function $0 \le r(z_j, z_i) \le 1$ (Fig. 6c, d) can be written in order to correlate the above quantities as,

$$\bar{u}_{i,j} = r(z_j, z_i) \cdot \bar{u}_i \tag{19a}$$

the value of the distributed "indirect" load acting along the generic cable *j* transmitted from the cable *i* can be expressed as:

$$q_{i,j} = q_i \cdot \frac{r^3(z_j, z_i) \cdot C_j}{\sum_{k=1}^{n} r^3(z_k, z_i) \cdot C_k} \quad \text{with} \quad C_j = \frac{64 \cdot E_j A_j}{3 l_j^4} \tag{19b}$$

The above relations can be obtained by writing the equilibrium condition for unit cable length $\sum_{j=1}^{n} q_{i,j} = q_i$, and the $n-1$ displacements relationships between the cable *i* and the remaining cables $j \neq i$:

$$\bar{u}_i^3 = \left[r(z_j, z_i) \cdot \bar{u}_j \right]^3 \qquad \text{with} \qquad j = 1,2,3,..,i-1,i+1,..,n \tag{20}$$

Eq. (20) correlates the value of the maximum displacement of the cable *i* with respect to the cable *j* by mean of the function $r(z_j, z_i)$. In other words, the above relations express the maximum deflection of the cable *i* by using the maximum deflection of the cable *j* multiplied by the influence function $r(z_j, z_i)$.

Therefore, since there exists a direct relation between the distributed load acting on a cable and its maximum displacement (Eq. (16)), the load acting on a generic cable can be obtained once its maximum deflection is known.

It can be observed that the function $r(z, z_i)$ is representative of the mechanical properties of the vertical 'equivalent' cables connecting the horizontal ones: in fact, if the net connected to the horizontal cables is very weak, when the cable *i* is displaced by a certain amount the displacements in the other connected horizontal cables would result as depicted in Figs 6c, d, with a rapid decrease of the displacements values for an increasing vertical distance from the cable *i*. On the other hand, in the case of a strong connecting net, the displacements of the cables would be as depicted in Fig. 6a, with a lower reduction effect as the vertical distance from the displaced cable *i* increases.

The governing equations (7) can be rewritten, using the above relations, as:

$$\frac{d^2 u_i}{dx^2} = -\frac{q_i - q_{ic} + q_{ci}}{H_i} = -\frac{q_i - \sum_{\substack{j=1 \\ j \neq i}}^{n} q_{i,j} + \sum_{\substack{j=1 \\ j \neq i}}^{n} q_{j,i}}{H_i} = \tag{21a}$$

$$= -\frac{\beta_i \cdot q_i \cdot \dfrac{r^3(z_i, z_i) \cdot C_i}{\sum_{k=1}^{n} r^3(z_k, z_i) \cdot C_k} + \sum_{\substack{j=1 \\ j \neq i}}^{n} \beta_j \cdot q_j \cdot \dfrac{r^3(z_j, z_i) \cdot C_i}{\sum_{k=1}^{n} r^3(z_k, z_j) \cdot C_k}}{H_i} = -\frac{Q_i}{H_i} \tag{21b}$$

$$\text{with} \quad H_i = \left(\frac{Q_i^2 \cdot l_i^2 \cdot E_i A_i}{24} \right)$$

that represents a system of nonlinear second order ordinary differential equations with $\bar{u}_j^3 = u_j^3(x = l_j/2)$, $\bar{u}_i^3 = u_i^3(x = l_i/2)$ and the coefficient β_j = 1.0 if $q_j \neq 0$ and $\beta_j = 0$ if $q_j = 0$. The last cited coefficient needs to be introduced in order to

take into account for the possibility that not all the cables are loaded at the same time.

It must be underlined as, in the above equations, any inertial effect is neglected since the mass of the retention barrier is very small and the horizontal acceleration of the cable and of the flowing material in contact with it can be supposed to be low during the whole loading process.

The above introduced function $r(z_j, z_i)$ can be reasonably assumed in the form:

$$r(z_j, z_i) = \frac{1}{\left(\left|z_j - z_i\right| + 1\right)^{m_{ji}}} \qquad \text{where} \qquad m_{ji} = \frac{-\ln(c)}{\ln\left(\left|z^* - z_i\right| + 1\right)} \tag{22}$$

in which $r(z^*, z_i) = c$ is the value attained by the function $r(z_j, z_i)$ at the vertical coordinate $z_j = z^*$ (i.e. for a cable placed at a relative distance from cable *i* equal to $d^*_i = \left|z^* - z_i\right|$) while the unit value of $r(z_j, z_i)$ is attained at $z_j = z_i$ (Fig. 7).

The assumed $r(z_j, z_i)$ indicates that the relation between the displacement of different horizontal cables depends on their relative vertical distance d_{ji} and on their reciprocal position. It can be observed that $m_{ji} \neq m_{ij}$ due to the non-linear force-displacement relationship (see Eqs (16) and (19b$_1$)). This is due to the difference between the relative displacement arising in cable *i* when cable *j* is subjected to a given displacement, and the relative displacements arising in cable *j* when cable *i* is subjected to the same displacement.

The function $r(z, z_i)$, if properly tuned through its coefficient m_{ij}, can represent the relation between the displacements of two connected cables.

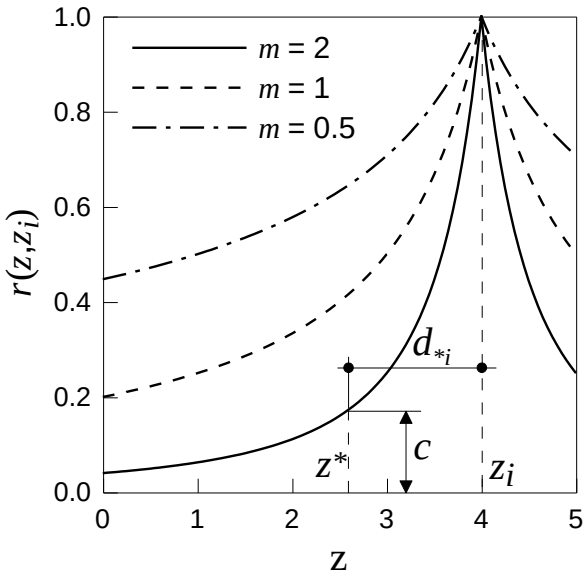

Fig. 7. Assumed pattern of the function $r(z_j, z_i)$ for different values of the exponent m and for $z_i = 4$ in Eq. (22).

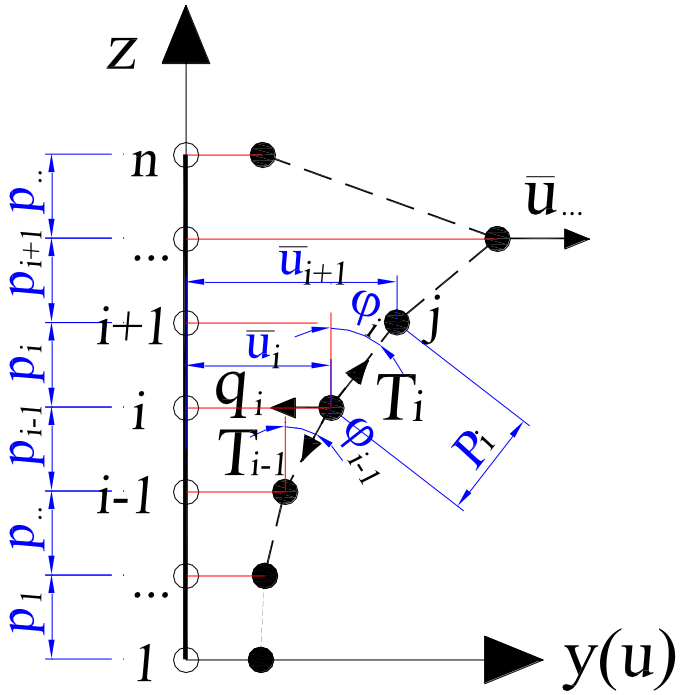

Fig. 8. Scheme of a vertical section of the barrier; the horizontal cables are represented by filled circles.

The determination of the function $r(z, z_i)$ can be achieved by considering the mechanical behaviour of the transversal midsection of the barrier (Fig. 8). The

equilibrium condition in the horizontal direction for the *i-th* cable can be written as:

$$q_i = T_i \sin\varphi_i - T_{i-1}\sin\varphi_{i-1} \tag{23}$$

$$\text{with} \quad \sin\varphi_i = \frac{\bar{u}_i - \bar{u}_{i-1}}{P_i}, \text{ and } \quad P_i = \sqrt{p_i^2 + \left(\bar{u}_i - \bar{u}_{i-1}\right)^2},$$

$$T_i = A_{ti}\cdot E_{ti}\cdot \varepsilon_i = A_{ti}\cdot E_{ti}\cdot \frac{\overbrace{P_i - p_i}^{\varepsilon_i}}{p_i} = A_{ti}\cdot E_{ti}\cdot \frac{\sqrt{p_i^2 + \left(\bar{u}_i - \bar{u}_{i-1}\right)^2} - p_i}{p_i}$$

where ε_i is the strain in the vertical cable connected to the horizontal cable *i*. On the other hand the relation between the applied load and the maximum transversal deflection of the cable is given by $q_i = (64\cdot E_i A_i / 3l_i^4)\cdot \bar{u}_i^{\,3}$ (see Eq.(16)). The above equilibrium equations (23) can thus be rewritten as:

$$\begin{aligned} q_i = \frac{64E_iA_i}{3l_i^4}\cdot \bar{u}_i^{\,3} = T_i\sin\varphi_i - T_{i-1}\sin\varphi_{i-1} = A_{ti}E_{ti}\cdot \frac{\sqrt{p_i^2 + \left(\bar{u}_i - \bar{u}_{i-1}\right)^2} - p_i}{p_i}\cdot \frac{\bar{u}_i - \bar{u}_{i-1}}{P_i} + \\ - A_{ti-1}E_{ti-1}\cdot \frac{\sqrt{p_{i-1}^2 + \left(\bar{u}_{i-1} - \bar{u}_{i-2}\right)^2} - p_{i-1}}{p_{i-}}\cdot \frac{\bar{u}_{i-1} - \bar{u}_{i-2}}{P_{i-1}} \end{aligned} \tag{24}$$

Eq. (24) simply states the equilibrium of the load acting on the cable under study and those deriving from the other connected cables, expressed by means of their maximum horizontal displacements.

Once the maximum transversal deflection $\bar{u}_k$ of the *k*-th cable is known, the maximum transversal deflections of the other cables can be obtained by the solution of the system of nonlinear equations (see Eq. (24)).

The solution of such a system is very awkward and does not allow an easy analytical treatment to get sought values. For such a reason the determination of the solution can be obtained through a numerical method; in the present paper an iterative evolutionary algorithm belonging to the Genetic Algorithm (GA) approaches is applied (Goldberg [46]; Gen and Cheng [47]).

In many physical problems, the solution of their mathematical formulation is often quite difficult to be determined by applying classical approaches. An increasing interest in a class of algorithms known as Genetic Algorithms (GAs), which operate by simulating the natural evolutionary processes of life - the Darwinian survival of the fittest principle is applied by iteratively improving the current

solution [46], [47], has been observed during last decades. Such algorithms represent random stochastic methods of global optimisation, and are used to minimise or maximise a chosen objective function suitable for a given problem. Genetic algorithms have successfully been applied to analyse several problems such as structural performance optimisation (Gantovnik et al. [48]; Brighenti [49]; Brighenti et al. [50]) and material design and parameters identification (Zohdi [51]) as well as several non-structural problems.

By using the above cited biological-based algorithm approach, the fulfilment of some conditions related to a desired objective function can be approximately imposed; in the present case the objective function to be minimised can be assumed to be represented by the total error e_{tot} in satisfying the equilibrium equations of the system (24), i.e.: $e_{tot} = \min$

$$
\begin{aligned}
& e_{tot} = \sum_{i=1}^{n} |e_i| \quad with \\
& e_i = \frac{64 E_i A_i}{3 l_i^4} \cdot \bar{u}_i^{\,3} - A_{ti} E_{ti} \cdot \frac{\sqrt{p_i^2 + \left(\bar{u}_i - \bar{u}_{i-1}\right)^2} - p_i}{p_i} \cdot \frac{\bar{u}_i - \bar{u}_{i-1}}{P_i} + \\
& + A_{ti-1} E_{ti-1} \cdot \frac{\sqrt{p_{i-1}^2 + \left(\bar{u}_{i-1} - \bar{u}_{i-2}\right)^2} - p_{i-1}}{p_{i-}} \cdot \frac{\bar{u}_{i-1} - \bar{u}_{i-2}}{P_{i-1}}
\end{aligned}
\tag{25}
$$

In Fig. 9 the flow-chart of the developed Genetic Algorithm used to minimize the errors expressed by Eq. (25) is reported. As can be observed, several initial random generations of the sought solution represented by the exponents m_{ij} are required (initial population made of *M* individuals). Performing the fitness evaluation of each individual (quantified through the violation of the equilibrium equations measured by e_{tot}), the highest ranking results can be identified and used for subsequent crossover and mutation operations to be carried out in order to get a new offspring of new individuals to be treated again as the previous one (Brighenti [49]; Brighenti et al. [50]). By repeating the above process, in an iterative way, up to the fulfillment of a given error tolerance, the numerical solution tends to the true solution of the problem.

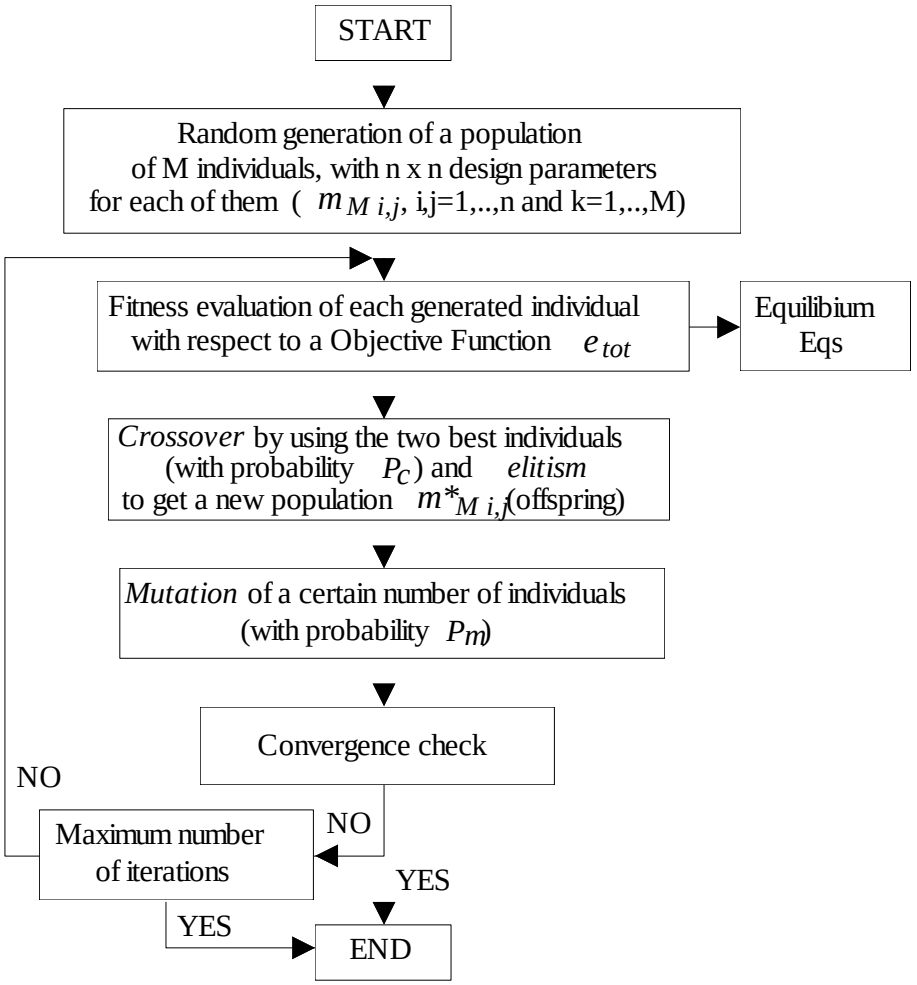

Fig. 9. Flow chart of the Genetic Algorithm used for the solution of the system given by Eqs (25).

As an example, the solution obtained by the GA in the case of 11 equally spaced cables having the same mechanical properties (cross section area, Young modulus and equal length) in which the sixth cable is displaced by a unit quantity ($\bar{u}_5 = 1$) is shown in Fig. 10.

It can be observed as the deformed pattern, obtained through the GA approach, is reasonably correct and that the corresponding exponent m_{j5} of the $r(z_j, z_5)$ law, evaluated for each couple of cables by considering the sixth cable as the reference one, is variable in the range 0.3-0.8 (see dashed line in Fig. 10).

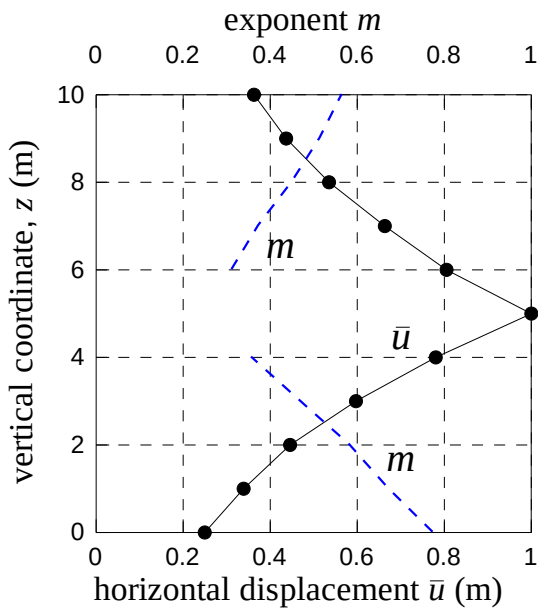

Fig. 10. Deformed pattern of 10 horizontal identical cables, joined by vertical cables, obtained through the GA; the corresponding exponent m of the $r(z_j, z_5)$ law (Eq. (22)) is also reported (dashed line).

It can be observed as the particular case of totally independent cables can be simulated by assuming $m_{ji} \to \infty$ in the expression of $r(z_j, z_i)$ (Eq. (22)); in such a particular case the differential equations become uncoupled and can be written as:

$$\frac{d^2 u_i}{dx^2} = -\frac{q_i}{H_i} \qquad i = 1,2,...,n, \tag{26}$$

with boundary conditions $u_i(0) = u_i(l_i) = 0$ and $L_i = \int_0^{l_i} \sqrt{1 + u_i'^2(x)}\, dx$

Finally, since the solutions of the equilibrium equations given by Eq. (8) can be observed to be characterised by the same patterns scaled by the value of the applied uniform load, the above Eqs (21) can be written by considering only the central maximum displacement for each cable, i.e.

$$\bar{u}_i = u_i(l_i/2) = \frac{\beta_i \cdot q_i \cdot \dfrac{r^3(z_i, z_i) \cdot C_i}{\sum_{k=1}^{n} r^3(z_k, z_i) \cdot C_k} + \sum_{\substack{j=1 \\ j \neq i}}^{n} \beta_j \cdot q_j \cdot \dfrac{r^3(z_j, z_i) \cdot C_i}{\sum_{k=1}^{n} r^3(z_k, z_j) \cdot C_k}}{2H_i} \cdot \frac{l^2}{4} = \frac{Q_i \cdot l_i^2}{8H_i} \tag{27}$$

In other words, the system of cables is assumed to be governed by n independent variables, $\bar{u}_i$, that is to say that every cable is completely described by one single parameter (degree of freedom) corresponding to its central and maximum horizontal displacement $\bar{u}_i$.

As a representative example, at the generic time instant *t* at which we assume to have $q_{t1}(t) \neq 0$, $q_{t2}(t) \neq 0$, $q_{t3}(t) \neq 0$, while $q_{t4}(t) = q_{t5}(t) = ... = q_{tn}(t) = 0$, in the case of cables having equal length l, cross section area A and elastic modulus E, the system of governing nonlinear equations becomes:

$$\begin{cases} \frac{8}{l^2}\bar{u}_1 = \frac{q_1}{H_1}\sum_{\substack{j=1\\ j\neq 1}}^{3}\frac{C_1^3 r^3(z_1,z_1)}{D_1} + \frac{C_1}{H_1}\sum_{\substack{j=1\\ j\neq 1}}^{3}\frac{q_j \cdot r^3(z_1,z_j)}{D_j} \\ \frac{8}{l^2}\bar{u}_2 = \frac{q_2}{H_2}\sum_{\substack{j=1\\ j\neq 2}}^{3}\frac{C_2^3 r^3(z_2,z_2)}{D_2} + \frac{C_2}{H_2}\sum_{\substack{j=1\\ j\neq 2}}^{3}\frac{q_j \cdot r^3(z_2,z_j)}{D_j} \\ \frac{8}{l^2}\bar{u}_3 = \frac{q_3}{H_3}\sum_{\substack{j=1\\ j\neq 3}}^{3}\frac{C_3^3 r^3(z_3,z_3)}{D_3} + \frac{C_3}{H_3}\sum_{\substack{j=1\\ j\neq 3}}^{3}\frac{q_j \cdot r^3(z_3,z_j)}{D_j} \\ \frac{8}{l^2}\bar{u}_4 = \frac{C_4}{H_4}\sum_{\substack{j=1\\ j\neq 4}}^{3}\frac{q_j \cdot r^3(z_4,z_j)}{D_j} \\ ..... \\ \frac{8}{l^2}\bar{u}_n = \frac{C_n}{H_n}\sum_{\substack{j=1\\ j\neq n}}^{3}\frac{q_j \cdot r^3(z_n,z_j)}{D_j} \end{cases} \quad \text{with} \quad C_i = \frac{64 \cdot EA}{3l^2 H_i}, \quad H_i = \left(\frac{Q_i^2 \cdot l^2 EA}{24}\right)^{1/3}, \quad D_j = \sum_{k=1}^{n} r^3(z_k, z_j) \cdot C_k \tag{28}$$

The solution vector $\mathbf{u}$ of the above system contains the maximum displacements of the cables, i.e. $\mathbf{u}^T = \{\bar{u}_1 \quad \bar{u}_2 \quad \bar{u}_3 \quad \bar{u}_4 \quad ... \quad \bar{u}_n\}$ at the time instant *t* at which the acting loads are considered.

The resulting system of non-linear differential equations (25) can be observed to be characterised by decoupled equations, since the effective coupling between the horizontal displacement is approximately accounted for by the relation given by Eq. (19a) which must be assessed from the value of the exponent *m*.

The above described mechanical model has been implemented in a simple in-house made Fortran code operating in two phases: i) determination of the function $r(z_j, z_i)$ (defined through the exponents m_{ij}) by the knowledge of the mechanical and geometrical characteristics of the horizontal cables and of the 'equivalent' vertical ones (representing the net) by using the Genetic Algorithm; ii) assessment of the displacements and forces in the deformed barrier in the time

domain (corresponding to the time interval of the debris impact on the structure), by using Eqs (8, 11, 13) calculated at discrete time intervals into which the total computation time has been subdivided. Obviously, the second phase of the calculation requires the evaluation of the external loads acting on the barrier (through Eqs (1-6)) throughout the entire duration of the debris flow phenomenon.

3.3. Modelling of the brake devices

As recalled at the beginning of the paper, real barriers are usually provided by brake system that enables to dissipate energy and to increase the cable length by allowing a beneficial reduction of the tension in the horizontal cables.
Usually, such devices becomes effective when the maximum tensile brake force is attained during the loading process; after that, the brake maintains such a maximum characteristic force and dissipates energy, up to the development of the maximum brake elongation. Once such maximum brake stroke is reached, the device loses its function and the force in the cable starts to increase again.
The force-displacement relationship for the brake device placed on the cable *i* can be written as:

$$f_b = \begin{cases} T_i \cong H_i & \text{if } T_i < f_{b,\max} \text{ and } s_b = 0 \\ f_{b,\max} & \text{if } T_i > f_{b,\max} \text{ and } s_b \le s_{b,\max} \\ T_i \cong H_i & \text{if } s_b > s_{b,\max} \end{cases} \tag{29}$$

where $f_b, f_{b,\max}, s_b, s_{b,\max}$ are the generic force, the maximum allowable brake force, the generic displacement and the maximum brake displacement, respectively. In order to take into account such a mechanical behaviour, the above formulated model can be modified as follows: i) check if the force in a generic cable reaches the maximum allowable brake force, $f_{b,\max}$; ii) if the previous condition is fulfilled (ie. $T_i > f_{b,\max}$) increase the cable length by a small fraction Δs_b of the original cable length in order to obtain the new effective cable length, $L_i = (l_i + \Delta s_b) \cdot (1 + H_i / E_i A_i)$; iii) determine again the force in the cable with such a new length by using Eqs (11, 12); iv) check whether the new force is lower than $f_{b,\max}$ otherwise go to step ii) and increase again the cable length.

Repeat the above procedure until the fulfilment of the condition $T_i < f_{b,\max}$ or continue without any other modification if the maximum brake elongation $s_{b,\max}$ has been reached.

Finally, the energy dissipated by the brake during its service can be easily obtained as:

$$E_b = f_{b,\max} \cdot s_b \tag{30}$$

4. Numerical applications, experimental validation and discussion

4.1. Parametric numerical examples

In the present section a representative example of retention barrier is considered and solved through the developed model, in order to simulate its mechanical behavior by varying some parameters of the barrier itself and of the debris flow. In particular, the effect of the stiffness of the net connecting to the horizontal cables and, for a given barrier configuration, the influence of the debris flow velocity v_0 are considered.

The parameters of the flowing debris and those of the barrier are the following: $k = 0.8$, $\alpha = 2.0$, $h_0 = 0.7m$, $\theta = 40^o$, $h_B = 5.0m$, $p = 1.0m$, $f_{b,\max} = 60kN, s_{b,\max} = 0.5m$ while the transversal cables representing the net have been assumed to be characterized by the 'equivalent' cross sectional area equal to the following values: $A_t = 0.5mm^2, 10mm^2, 50mm^2, 200mm^2$. In order to investigate the effect of the debris flow velocity (by assuming for such a case $A_t = 0.5mm^2$), the following values have been considered: $v_0 = 2.0m/s, 4.0m/s, 8.0m/s$. The geometry of the barrier is reported in Fig. 11a (the cable No 1 located at $z = 0$ is assumed to be fixed, i.e. it does not undergo any significant displacement), while in Fig. 11b the scheme of the so-called drag force f_d – occurring when the allowable volume for the debris accumulation is completely filled by the flowing material – is represented when the flow continues to take place above the barrier.

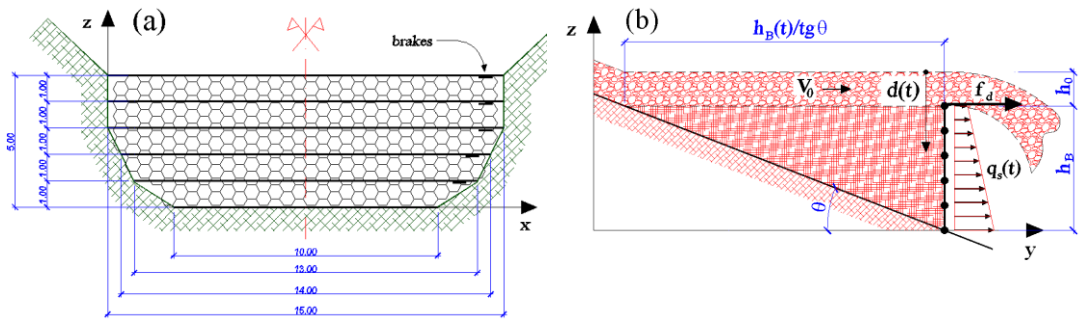

Fig. 11. Geometrical dimensions of the considered barrier (a) and scheme of the drag force occurring when the debris flow continues above the barrier (b) (dimensions are expressed in m).

In Fig. 12 the effect of the different values of the cross section of the vertical cables in presented. In particular in Fig. 11a the maximum tensile force in the cable during the whole impact period of the debris against the barrier is presented; as can be noted the maximum tensile force reduces by increasing the stiffness of the net and such a maximum force becomes almost identical for all the cables. On the other hand, for a weak net the cables are subjected to very different maximum force values which are also higher than those calculated with strongest nets. The case of a barrier without brakes (with $A_t = 50mm^2$) is also reported; the forces in the cables are obviously much higher than those obtainedfor the same barrier with the brakes.

In Fig. 12b the energy dissipated by all the brakes during the impact is represented. As it can be noticed, the total final amount of dissipated energy decreases when the net stiffness increases since the forces occurring in the cables are lower when the net is stiffer and therefore the brakes do not reach their final allowable stroke. In Fig. 12c, d the total elastic energy stored in the barrier and the sum of the total elastic and dissipated energy are represented vs time, respectively. The trend shown by the curves for different net stiffness is in accordance with the forces developing in the cables during the phenomenon. It can be also observed that, after reaching the complete filling of the barrier (see Fig. 11b), the phenomenon reaches a steady state and the above quantities remain constant with time.

In Fig. 13 the deformed pattern of the barrier at the time t=1s is represented for the four different transversal nets; it is apparent, once again, the load distribution effect of the transversal net on the horizontal cables of the barrier.

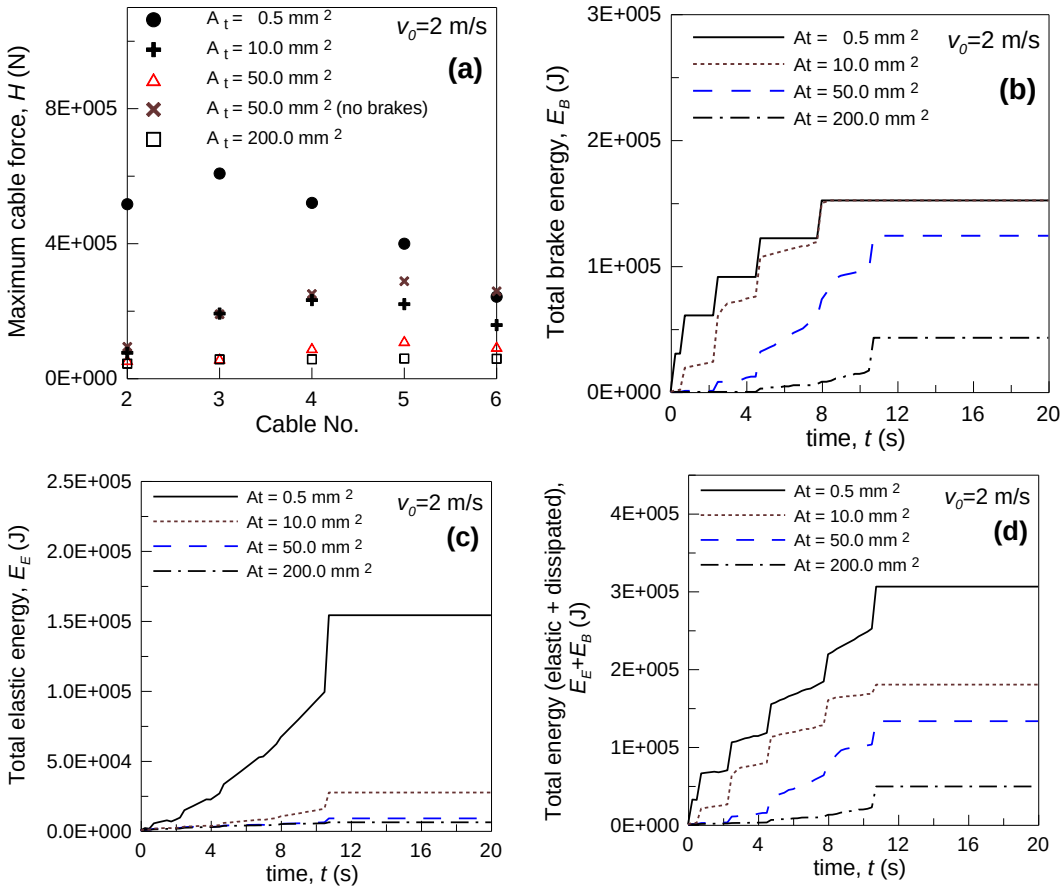

Fig. 12. Barrier with different stiffness of the superposed steel net: maximum tensile force in the cables (a), dissipated brake energy of the barrier (b), elastic energy of the barrier (c) and total (elastic + dissipated) energy of the barrier (d) vs the time t.

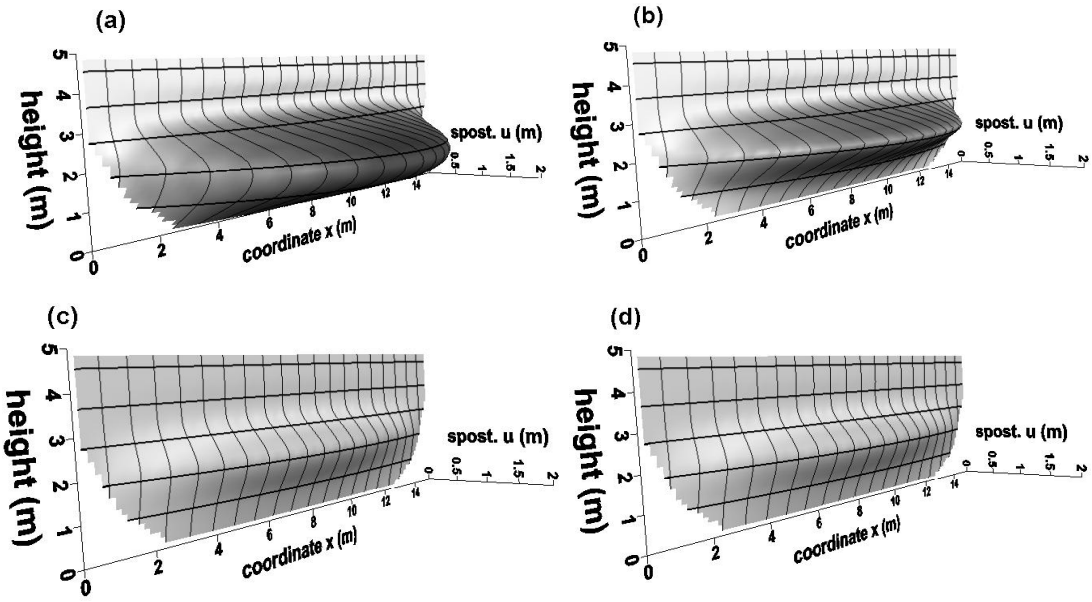

Fig. 13. Deformed pattern of the barrier with different stiffness of the superposed steel net at the time t=1s: case of $A_t = 0.5mm^2$ *(a),* $A_t = 10mm^2$ *(b),* $A_t = 50mm^2$ *(c) and* $A_t = 200mm^2$ *(d).*

Finally the effect of the debris flow surges velocity is herein considered. In Fig. 14 the maximum tensile force attained in the different cables of the barrier is represented for the three assumed debris flow surges velocity ($v_0 = 2.0m/s, 4.0m/s, 8.0m/s$). It appears as the force in the bottom cable (No. 2) is not influenced by v_0 since the static load produced by the accumulated material prevails over the dynamic force; on the other hand, the velocity influence becomes relevant for the cables placed at higher levels. In Fig. 14b the total amount of dissipated energy is represented; it appears that such total energy at the end of the phenomenon is the same for the different velocities since all the brakes reach their maximum allowable sliding length. In the case of higher velocities of the flow surges, the maximum brakes displacement is reached in a shorter time with respect to lower velocities.

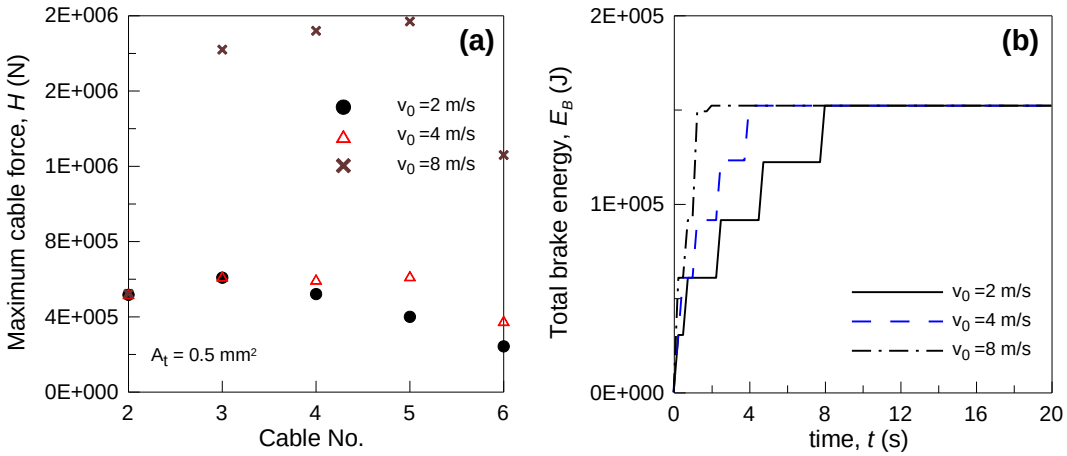

Fig. 14. Effect of the debris flow velocity. Maximum tensile forces in the cable during the debris impact (a) and total energy dissipated by the brakes vs the time t (b) for different values of v_0.

4.2. Simulation of a full scale test of a retention barrier

In order to assess the reliability of the proposed analytical model, the simulation of a full scale test on a barrier is considered hereafter.

The test was carried out inside a limestone quarry located in the Pieve d'Alpago district (Belluno province, Northeastern Italian Alps); the artificial channel was built by re-shaping an existing natural impluvium and the barrier was located at its bottom (Fig. 4). The obtained artificial channel was 2 m large and 48 m long, with an average slope of 40°. The material used to simulate the flow was constituted by well-graded limestone blocks with diameter ranging from few cm to 1.5 m. Due to the particular geometry of the channel, to the nature of the material and to the machinery used to mobilize it, it was not possible to keep the material saturated; however, the effects on the barrier in terms of deformation and forces were in good agreement with other small scale and large scale test results available in bibliography (Davies [52], Iverson [53], Canelli [41]).

During the test, both deformation and horizontal cable forces were measured using photogrammetric techniques and load cells, respectively. The photogrammetric restitution was based on the pictures taken by a couple of frontal high definition camera that shot at a speed of 23 frame per second. The load cells, with a maximum measurement range of 1000 kN, were mounted on each of the

five horizontal cables as depicted in Figure 2 and their data were recorded at1Hz frequency.

The registered flow velocity was 2.51 m/s on average with measured peaks of 9 m/s, the total volume stopped at the barrier was of approximately 400 m^3, the average flow height h_0 was equal to 0.7 m while the material density was estimated in 1790 kg/m^3. The test came to the end with the filling up of the whole barrier, no overflow was allowed in order to preserve the safety at test site.

The structure under consideration is characterized by an average span of about 17.00 m while its height is equal to 4.00 m; it is composed by four main horizontal double steel cables (6x19 class according to UNI EN 12385-4) having diameter ϕ20 mm, fixed at the extremities to foundations grouted inside the channel shoulders. The four horizontal main cables are mounted at a relative vertical distance *p* equal to about 1.33 m (Fig. 2). A steel ASM 3-4- 350/200 ring net made by ϕ350 mm rings, connected at four point contact is linked at the horizontal cables (Fig. 3). The rings are formed by a single steel wire (1380 N/mm^2 minimum tensile strength) having a diameter ϕ 3 mm and rolled up in 10 loops and 2 spirals. The lower cable was fixed at the bottom surface of the channel in the real test, by means of several anchors; in order to account for the effect of those restrains in the analytical model, since the proposed simplified analytical model does not allow the application of restrain along the main cables, a cable with a larger cross sectional area (20 times the area of the others) was adopted. This assumption implies that the horizontal displacements of the lower cable are negligible and its calculated axial forces are omitted for the comparison between real case and numerical results.

The analytical model has been solved by assuming $\alpha = 1.5$, $k = 0.5$ to describe the loads on the barrier; the value of the empirical coefficient α and of the earth pressure coefficient *k* were recovered through back analysis, considering the indications of Canelli et al. [41] and Bugnion et al. [54] while the exponent *m* of the functions $r(z_j, z_i)$ relating each cable with the others - i.e. for the assessment of the cables interaction - have been calculated according to the above described GA procedure.

The values of the coefficients necessary for the evaluation of the forces induced by the debris flow against the barrier (Eqs 1, 3), have been performed by following the considerations below.

Bugnion et al. [54] have performed several tests of flow against obstacles and computes the α value. They shows that 2 is the maximum value. For this reason the Authors considered this value in the initial phase of development of the work. For the coefficient of earth pressure *k*, the value *k* = 0.5 was chosen because Kwan and Cheung [40] suggested a maximum value of 1 in undrained condition but we could observe a condition of partial saturation during the flow and of good drainage during the impact of the debris against the barrier. Therefore, the friction angle of the debris accumulation behind the barrier was originally assumed between 20° and 30°, converging to the value of 20° through a back analysis procedure developed in order to better fit the experimental results.

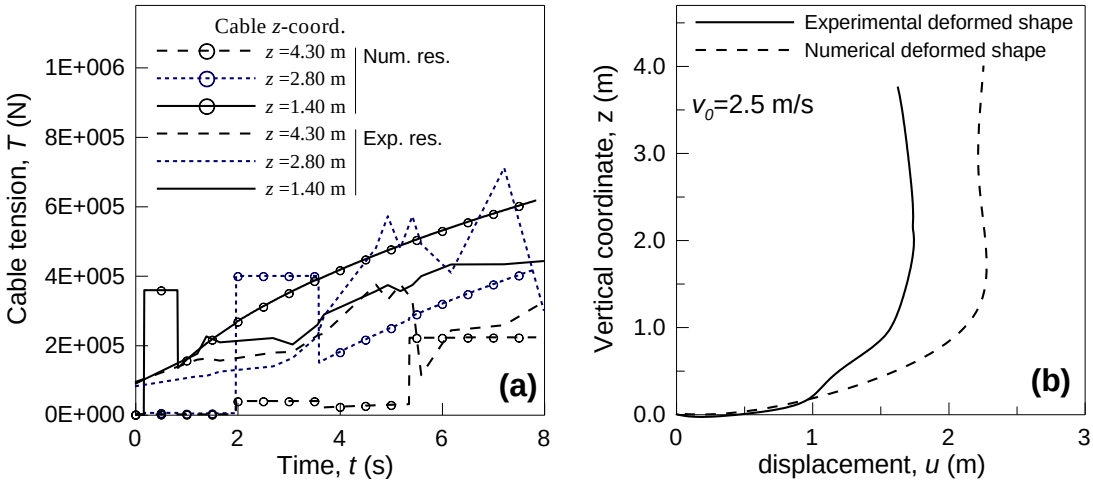

Fig. 15. Comparison between experimental and analytical results of: (a) tension forces in the horizontal structural cables vs. time; (b) maximum deformed shape of the barrier at the midspan vertical section.

In Fig.15 (a) the forces measured in each cable (identified through its co-ordinate position *z*) during the test are plotted against time, together with those determined using the proposed analytical model. In Fig. 15 (b) are reported both the shape of the deformed barrier measured at the central vertical section at the end of the test and that calculated using the proposed model. Although some differences between experimental and numerical results were obtained, especially for what it concerns the barrier deformation, the induced state of traction in the cables are in good agreement. This is possibly due to the initial state of stress in the cables, which is originally applied during the structure assembly; this pretension is not influencing the final state of stress induced by the debris flow impact while it

does, instead, influence its deformation particularly at the beginning and at the end of the loading process. Furthermore, the lower portion of the barrier (lower horizontal cable) is free to deform along its length in the proposed model (its displacement is fictitiously limited by adopting a cable cross section area greater than its effective value, as already discussed) while, in the real case, is fixed at the channel surface by means of eyebolts. These boundary conditions can be reconsidered and improved in future development of the work.

Regarding the duration of the test reported in abscissa in Fig. 15 (a), it should be considered that, while in the analytical model it is calculated using the geometry of the channel and the velocity of the debris surge, for what it concerns the real test it is determined considering the debris flow as if it was flowing at a constant rate, neglecting the interruptions that occurred between surges due to the above described operational limitations.

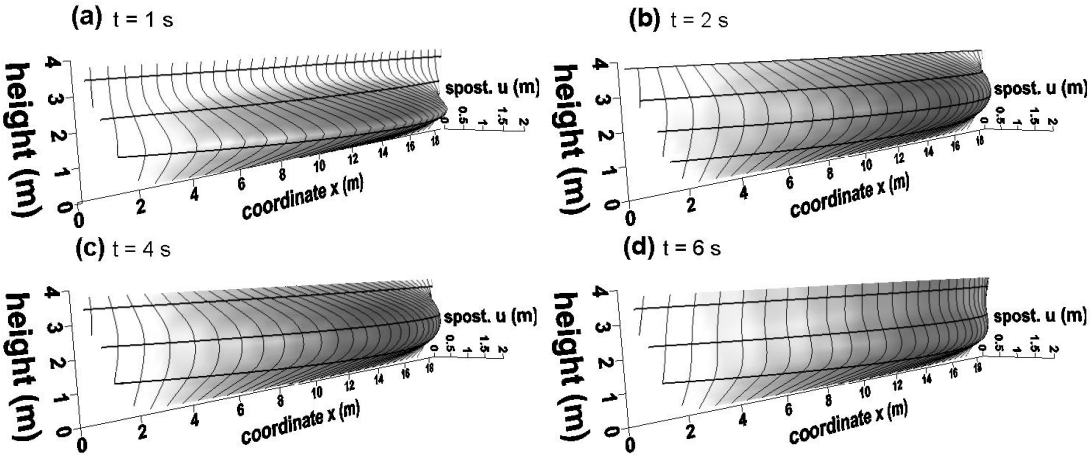

Fig. 16. Deformed patters provided by the present model for t=1.0 s (a), t=2.0 s (b), t=4.0 s (c) and t=6.0 s (d) (see Fig. 15b) corresponding to the simulation of the on site tests described above.

In Fig. 16 a full 3-dimensional reconstruction of the net deformed pattern during the loading process is also given; as can be observed it shows how the method can realistically reproduce the barrier deformation with the time, providing the net shape as the flow phenomena proceeds and the debris accumulates behind the retention barrier. This results can be usefully applied in the future for setting up a real time net monitoring system able to define threshold values to be controlled in situ by means of specific measuring devices.

The energy dissipated by the barrier upon the impact with the debris flow can be calculated by adding two terms: the first derived from the dissipation of the brake devices E_b and the second induced by the elastic deformation of the supporting cables E_E (see Eq. (31)).

$$E_b = f_{b,\max} \cdot s_b, \qquad E_E = 1/2(LH^2/EA) \tag{31}$$

In our simulation of the test, the amount of energy dissipated at the end of the impact phase is approximately equal to 286 kJ.

Sun & Law [55] proposed several analytical solution for the determination of the design impact energy of the barrier based upon pile-up or run-up mechanisms. In our case, the most appropriate formulation appears to be the run-up mechanism with the height of the final debris accumulation equal to the height of the barrier. The related equation, proposed by Sun & Law [55] and rewritten with our notations becomes:

$$E_B = \frac{\rho_d \, Fr \, v_0 \, h_b^2}{4 h_0 \tan(\theta+\alpha)} - \frac{\rho_d \, g \, Fr \, h_b^3}{3 h_0 \, v_0 \tan(\theta+\alpha)\sin(\theta+\alpha)}(\sin\alpha + \mu\cos\alpha) \tag{32}$$

The application of Eq. (32) to the Pieve d'Alpago test, considering the parameters acquired from the back analysis described above, gives a design impact energy of the barrier E_B equal to 452 KJ. This result is obtained considering the angle between the horizontal and the upper surface of the debris accumulated behind the barrier substantially horizontal (α = 1°) as observed during the test. The interface friction coefficient μ is determined, using Eq. (33) described in [55] through a back analysis procedure aimed at obtaining the impact duration T_f comparable with that calculated by the proposed analytical model (approximately 8 s).

$$T_f = \frac{h_b^2}{2 v_0 \, h_0 \tan(\theta+\alpha)} \tag{33}$$

The above consideration indicates that around 37% of the design impact energy of the debris flow is dissipated internally during the impact phase and only the remaining portion is transferred to the barrier.

5. Conclusions

The energy associated with debris flows along with their velocity, active volumes and run out distances have often made these phenomena very destructive and dangerous. The design of retention devices, which are often a must in populated area or wherever it is necessary to limit the destructive effects of debris flows, is often carried out using previous experiences and subjective knowledge of the phenomena mechanics. Analytical approaches are seldom used and generally based on numerical modelling (FEM). However, the numerical modelling of these structures, which should be carried out considering the debris flow impact dynamics, can turn out to be very complicated and not always reliable in applicative cases. For these reasons, the need of a sound design instrument, easily applicable in standard, is becoming of paramount importance and is not yet available to practitioners.

In the present paper a simplified analysis of the mechanics of debris-flow is considered in order to estimate the forces developed by such a flow impacting on a retention barrier. Then, an analytical simplified structural model of cable-like retention barriers is developed, based on the equation of equilibrium of wires under large displacements condition, and the restraining forces as well as the cable stresses are finally estimated. A parametric study has been presented, in order to demonstrate the capability of the proposed model to capture all the main mechanical aspect occurring during the impact of a debris flow against a flexible structure. The boundary conditions for the lower cable are the same as those listed for the other cables (i.e. anchored at the channel sides), avoiding to consider the lower cable connected to the channel bottom. This geometrical configuration is often used, in consideration of the scarce mechanical reliability of the debris deposited along the channel.

The comparison between experimental and numerical results has been presented, as well. The satisfactory agreement hereby shown, enable us to state that the present approach is promising, even though, some differences have been recorded; such discrepancies are possibly due to the simplifying variables introduced in the calculation and to some of the theoretical assumption needed to achieve an analytical solution of the problem. However, this work represents a starting point that will need further development along with additional validations. At present, new experimental data are processed (either taken from literature or from direct

measurements) and several parametric analysis are under development in order to define the sensitivity of the model upon changes in the structural geometry or in the debris flow features.

Acknowledgements

The authors gratefully acknowledge the research support for this work provided by the Italian Ministry for University and Technological and Scientific Research (MIUR) and by the ICE (Institute for Foreign Commerce). We also wish to acknowledge the financial and technical support of Consorzio Triveneto Rocciatori S.C.r.l. and Officine Macaferri S.p.a. (Italy).

References

[1] Takahashi T (1983) Debris flow and debris flow deposition. In: Advances in the Mechanics and Flow of Granular Materials, Vol. II. Shahinpoor M. (ed.) Trans. Tech. Publ. 57–77.

[2] Govi M, Mortara G, Sorzana PF (1985) Eventi Idrogeologici e Frane, Geologia Applicata e Idrogeologia, Vol. XX, Part II, 359–375.

[3] Pierson TC, Costa JE (1987) A rheologic classification of subaerial sedmit-water flow. Geol. Soc. Am., Rev. Eng. Geol. 7: 112.

[4] Costa JE (1984) Physical geomorphology of debris flows. In J.E. Costa & P.J. Fleisher (eds), Developments and Applications of Geomorphology. New York, Springer-Verlag: 268–317.

[5] Phillips CJ, Davies TRH (1991) Determining rheological properties of debris flow material. Geomorphology 4: 101–110.

[6] Meunier M (1991) Eléments d'hydraulique torrentielle. CEMAGREFEtudes, Série Montagne, n. 1: 278.

[7] Wan Z, Wang Z (1994) Hyperconcentrated Flows, IAHR Monograph Series, Balkema, Rotterdam.

[8] Coussot P., Meunier M. (1996) Recognition, classification and mechanical description of debris flows. Earth-Science Reviews 40: 209–227.

[9] Hungr O, Evans SG, Bovis MJ, Hutchinson JN (2001) A review of the classification of landslides of the flow type. Environmental and Engineering Geoscience 7(3): 221–238.

[10] Takahashi T (2007) Debris flow. Mechanics, Prediction and Countermeasures. Taylor and Francis/Balkema: 33-157 & 211-254

[11] Okuda S, Suwa H, Okunishi K, Yokoyama K, Nakano M (1980) Observations on the motion of a debris flow and its geomorphological effects. Zeitschrift für Geomorphologie N.F., Suppl. Bd., 35: 142–163.

[12] Marchi L, Arattano M, Deganutti M (2002) Ten years of debris-flow monitoring in the Moscardo Torrent (Italian Alps). Geomorphology 46 (1/2): 1–17.

[13] Hürlimann M, Rickenmann D, Graf C (2003) Field and monitoring data of debris-flow events in the Swiss Alps. Canadian Geotechnical Journal 40 (1): 161–175.

[14] Tecca PR, Deganutti AM, Genevois R, Galgaro A (2003) Velocity distribution in a coarse debris flow. In Debris-flow hazard mitigation: Mechancis, Prediction and Assesment. Proc. of the 3rd Int. DFHM Conference. Davos, CH. Sept. 10-12, 2003. D. Rickenmann & C.L. Chen (eds). Rotterdam, Millpress: 905–916.

[15] Iverson RM (1997) The physics of debris flows. Review of Geophysics 35, 3:45–296.

[16] Mizuyama T, Uehara S (1983) Experimental study of the depositional process of debris flow. Japanese Geomorphological Union 4 (1): 49–63.

[17] Liu GR, Lee FC, Tsai HP (1997) The flow and impact force on a debris dam. Debris-flow Hazards Mitigation, ASCE, New York: 737–746.

[18] Chau KT, Chan LCP, Luk ST, Wai WH (2000) Shape of deposition fan and runout distance of debris-flow: effects of granular and water contents. In "Debris-Flow Hazards Mitigation: Mechanics, Prediction and Assessment". Rotterdam, Wieczorek & Naeser (eds) Balkema: 387–395.

[19] Deganutti AM, Tecca PR, Genevois R, Galgaro A (2003) Field and laboratory study on the deposition features of a debris flow. In D. Rickenmann & C.L. Chen (eds), Debris-flow Hazards Mitigation: Mechanics, Prediction, and Assessment; Proceedings of the 3rd International DFHM Conference. Davos, Switzerland, Sempt. 10-12, 2003. Rotterdam, Millpress: 833–841.

[20] Ghilardi P, Pagliardi M, Zanittigh B (2006) Analisi sperimentale del processo di impatto di miscele granulari sature contro pareti verticali. XXX Convegno di Idraulica e Costruzioni Idrauliche, IDRA 2006.

[21] Major J. J. (1997) Depositional Processes in Large Scale Debris Flow Experiments. The Journal of Geology. Vol. 105, No. 3, May 1997,pp. 345-366

[22] Ferrero A M, Giani G P, Segalini A (2010) Numerical and experimental analysis of debris flow protection fence efficiency. Proc. European Rock Mechanics Symposium (Eurock 2010), Lausanne, CH. Balkema, Rotterdam: 578-578

[23] Olivares L, Picarelli L (2001) Susceptibility of loose pyroclastic soils to static liquefaction: some preliminary data, in: Proc. Of Int. Conf. on Landslides – Causes, Impacts and Countermeasures, Davos, 75–85.

[24] Hungr O, Evans SG (1996) Rock avalanche runout prediction using a dynamic model. In: Senneset, K. (Ed.), Proc. of the 7th International Symposium on Landslides, Trondheim. A.A. Balkema, Rotterdam, 233–238.

[25] Pirulli M (2005) Numerical modelling of landslide runout, a continuum mechanics approach. PhD Thesis, Department of Structural and Geotechnical Engineering, Politecnico di Torino, Italy.

[26] Vallance JW (1994) Experimental and field studies related to the behaviour granular mass flows and the characteristics of their deposits. Ph.D. thesis, Michigan Technological University.

[27] Cesca (2008) Debris-flow runout predictions based on the average channel slope (ACS) Original Research Article Engineering Geology, Volume 98, Issues 1–2, 21 April 2008, 29–40.

[28] Bagnold RA (1954) Experiments on a gravity-free dispersion of large solid spheres in a Newtonian fluid under shear Proc. R. Soc. Lond. A, 225: 49–63.

[29] Goldhirsch I (2003) Rapid Granular Flows, Annual Review of Fluid Mechanics 35: 267–293.

[30] Jenkins JT, Hanes DM (1998) Collisional sheet-flow of sediment driven by a turbulent fluid. J. Fluid Mech. 370: 29–52.

[31] Hanes DM, (1998) Collisional sheet flows of sediment driven by a turbulent fluid. Fluid Mechanics 370: 29–52.

[32] Armanini A, Fraccarollo L, Larcher M (2008) Liquid-granular channel flow dynamics. Powder Technology 18, 2: 218–227.

[33] Chen H, Lee CF (2000) Numerical simulation of debris flows. Canadian Geotechnical Journal 37, 1: 146.

[34] Denlinger RP, Iverson RM (2004) Granular avalanches across irregular three-dimensional terrain: 1. Theory and computation.3 J. of Geophysical Res. 109: F01014: 14.

[35] McDougall S, Hungr O (2004) A model for the analysis of rapid landslide motion across three-dimensional terrain. Canadian Geotechnical Journal 41, 1084–1097.

[36] Savage SB, Hutter K (1989) The motion of a finite mass of granular material down a rough incline. J. of Fluid Mechanics 199: 177–215.

[37] Suwa H, Okuda S (1983) Deposition of debris flows on a fan surface, Mt. Yakedake, Japan. Z. Geomorphol. Suppl. 46: 79–101.

[38] Hungr O (1985) A model for the runout analysis of rapid flow slides, debris flows, and avalanches. Can Geotech J. 32: 610–623.

[39] Van Dine DF (1996) Debris Flow Control Structures for Forest Engineering. Province of British Columbia Ministry of Forests Research Program, 68.

[40] Kwan J.S.H. & Cheung R.W.M. (2012) Suggestion on Design Approaches for Flexible Debris-resisting Barriers . Standard and Testing Division. Discussion Note DN1/2012. The Government of Hong Kong Special Administrative Region.

[41] Canelli L., Ferrero A.M., Migliazza M., Segalini A. (2012) Debris flow risk mitigation by the means of rigid and flexible barriers – experimental tests and impact analysis. Nat. Hazards Earth Syst. Sci., 12, 1–7 (www.nat-hazards-earth-syst-sci.net/12/1/2012/ doi:10.5194/nhess-12-1-2012).

[42] WSL (2009) Full-scale Testing and Dimensioning of Flexible Debris Flow Barriers. Swiss Federal Institute for Forest, Snow and Landscape Researc (WSL), 22 p.

[43] Lo D.O.K. (2000) Review of natural terrain landslide debris-resisting barrier design. Geotechnical Engineering Office Report No. 104. The Government of Hong Kong Special Administrative Region: 14-32.Major JJ (1997) Depositional processes in large-scale debris-flow experiments. The Journal of Geology 105: 345–366.

[44] Seidel M. (2009) Tensile Surface Structures: A Practical Guide to Cable and Membrane Construction, Wiley.

[45] Levy R, Spillers WR (2004) Analysis of Geometrically Nonlinear Structures, Kluwer Academic Publishers, 2nd ed.: 151–186

[46] Goldberg DE (1989) Genetic algorithms in search, optimization, and machine learning. MA, Addison-Wesley Publishing Company inc: 1-56.

[47] Gen M, Cheng R (1996) Genetic algorithms and engineering design. New York, John Wiley and Sons:1:40

[48] Gantovnik VB, Anderson-Cook CM, Gürdal Z, Watson LT (2003) A genetic algorithm with memory for mixed discrete-continuous design optimization. Comp. & Struct. 81: 2003–2009.

[49] Brighenti R (2005) Fibres distribution content optimisation in fibre-reinforced composite by a genetic algorithm. Int. J. Composite Structures 71(1): 1–15.

[50] Brighenti R, Carpinteri A, Vantadori S (2006) A genetic algorithm applied to optimisation of patch repairs for cracked plates. Comp. Meth. App. Mech. and Engng. 196: 466–475.

[51] Zohdi TI (2003) Constrained inverse formulations in random material design, Comp. Meth. Appl. Mech. Engng 192: 3179–3194.

[52] Davies T.R.H. (1988) Debris flow surges – a laboratory investigation. Mitteilung Nr. 96, VAW, ETH-Zurich, Switzerland.

[53] Iverson, R. M., J. E. Costa, and R. G. LaHusen (1992), Debris-flow flume at H. J. Andrews Experimental Forest, Oregon, U.S. Geol. Surv. Open File Rep., 92-483, 2 pp. (Available at http://vulcan.wr.usgs.gov/Projects/MassMovement/Publications/OFR92-483/framework.html)

[54] Bugnion L, McArdell B.C., Bartelt P, Wendeler C. (2012) Measurements of hillslope debris flow impact pressure on obstacles. Landslides. 9:179-187. DOI 10.1007/s10346-011-0294-4

[55] Sun H.W. & Law R.P.H (2012) A preliminary study on impact of landslide debris on flexible barriers. Geotechnical Engineering Office. Standard and Testing Divison. Technical Note 1/2012. The Government of Hong Kong Special Administrative Region.